Monthly Notices
of the
ROYAL ASTRONOMICAL SOCIETY

Mon. Not. R. Astron. Soc. **416,** 2174–2181 (2011) doi:10.1111/j.1365-2966.2011.19194.x

The luminosity function of *Swift* long gamma-ray bursts

Xiao-Feng Cao,[1] Yun-Wei Yu,[1,2]★ K. S. Cheng[2] and Xiao-Ping Zheng[1]

[1]*Institute of Astrophysics, Central China Normal University, Wuhan, 430079, China*
[2]*Department of Physics, The University of Hong Kong, Pokfulam Road, Hong Kong, China*

Accepted 2011 June 6. Received 2011 May 30; in original form 2010 December 4

ABSTRACT

The accumulation of *Swift* observed gamma-ray bursts (GRBs) has gradually made it possible to directly derive a GRB luminosity function (LF) from the observational luminosity distribution. However, two complexities are involved: (i) the evolving connection between GRB rate and cosmic star formation rate; and (ii) observational selection effects due to telescope thresholds and redshift measurements. With a phenomenological investigation of these two complexities, we constrain and discriminate two popular competing LF models (i.e. the broken-power-law LF and the single-power-law LF with an exponential cut-off at low luminosities). As a result, we find that the broken-power-law LF may be more favoured by observations, with a break luminosity $L_{\rm b} = 2.5 \times 10^{52}\,{\rm erg\,s^{-1}}$ and prior- and post-break indices $\nu_1 = 1.72$ and $\nu_2 = 1.98$. Regarding an extra evolution effect expressed by a factor $(1+z)^{\delta}$, if the metallicity of GRB progenitors is lower than $\sim 0.1\,{\rm Z}_{\odot}$ as expected by some collapsar models, then there may be no extra evolution effect other than the metallicity evolution (i.e. δ approaches zero). Alternatively, if we remove the theoretical metallicity requirement, then a relationship between the degenerate parameters δ and $Z_{\rm max}$ can be found, very roughly, $\delta \sim 2.4(Z_{\rm max}/{\rm Z}_{\odot} - 0.06)$. This indicates that extra evolution could become necessary for relatively high metallicities.

Key words: gamma-ray burst: general.

1 INTRODUCTION

Some confirmed associations between gamma-ray bursts[1] (GRBs) and Type Ib/c supernovae (Stanek et al. 2003; Hjorth et al. 2003; Chornock et al. 2010) robustly suggest that GRBs are powered by the collapse of the cores of massive stars, which is also widely accepted in theory (Woosley 1993; Paczyński 1998; Fryer, Woosley & Hartmann 1999; Wheeler et al. 2000; Woosley & Bloom 2006). In other words, the detection of each GRB provides a witness to the death of a massive star. Moreover, the intense brightness of GRBs makes them detectable even at the edge of the Universe (the highest redshift of GRBs is ∼9.4 as reported by Cucchiara et al. 2011). So GRBs can in principle be used as a tracer of the cosmic star formation history. The crucial problem is whether GRBs are an unbiased tracer or, more directly, how to calibrate the GRB event rate to the star formation rate (SFR). On the one hand, the cosmic evolution of metallicity could be involved. This is because a very high angular momentum is required for GRB progenitors and meanwhile massive stars in lower-metallicity environments are less likely to lose much angular momentum through stellar winds (e.g. Meynet et al. 1994; Langer & Henkel 1995; Vink & de Koter 2005; MacFadyen & Woosley 1999; Woosley & Heger 2006). On the other hand, the luminosity function (LF) of GRBs can also play an important role in the conversion from the observed GRB redshift distribution to the GRB formation history, since the luminosity selection by telescopes leads to a lower detection probability for higher-redshift GRBs.

To derive a GRB LF directly was impossible before the launch of *Swift* (Gehrels et al. 2004), since there were only a few GRBs whose redshifts had been measured. A possible alternative method invokes some luminosity-indicator relationships to avoid redshift measurements (e.g. Fenimore & Ramirez-Ruiz 2000; Yonetoku et al. 2004; Firmani et al. 2004), but the robustness of those indicators may not be high enough. A much more popular method is to assume a LF form with a few model parameters and then to fit the flux distribution of the observed GRBs ($\log N - \log P$ distribution; Schmidt 1999; Porciani & Madau 2001; Firmani et al. 2004; Guetta, Piran & Waxman 2005; Natarajan et al. 2005; Daigne, Rossi & Mochkovitch 2006; Salvaterra & Chincarini 2007; Salvaterra et al. 2009; Campisi, Li & Jakobsson 2010). Correspondingly, before *Swift*, a very large sample of GRBs had been provided by the Burst and Transient Source Experiment (BATSE) on board the *Compton Observatory*. Nevertheless, by such a fit to the $\log N - \log P$ distribution only, it is not easy to eliminate the degeneracy among the model parameters and even to determine the form of the LF. As a result, two

★E-mail: yuyw@phy.ccnu.edu.cn

[1] Throughout we refer only "long" gamma-ray bursts with $T_{90} > 2$ s, where T_{90} is the interval observed to contain 90 per cent of the prompt emission.

competing LF models, a broken power law (BPL) and a single power law with an exponential cut-off (SPLEC) at low luminosities, are usually adopted in the literature.

Thanks to the *Swift* spacecraft, in the past few years the number of GRBs with measured redshift has grown rapidly. This makes it possible to provide more stringent constraints on the LF parameters (Daigne et al. 2006; Salvaterra & Chincarini 2007; Salvaterra et al. 2009; Campisi et al. 2010). The new constraints robustly rule out the models in which GRBs are unbiased tracers of the cosmic star formation or GRBs are characterized by a constant LF. In other words, an evolution effect is suggested. In view of the large size of the *Swift* GRB sample, it has become possible to derive a GRB LF only with *Swift* GRBs. Very recently, Wanderman & Piran (2010) tried to convert the luminosity distribution of *Swift* GRBs directly to a LF, without a prior assumed LF form and without help from the BATSE data. In such a LF determination process, the treatment of observational selection effects plays a very important role. Meanwhile, much attention should also be paid to a possible extra evolution effect. In this paper, with a phenomenological investigation of the evolution effect and the selection effects, we constrain and discriminate the BPL and SPLEC models by using *Swift* observed GRBs.

In the next section, some observational and theoretical considerations related to the GRB LF are described. In Section 3, the evolution effect is constrained and analysed with relatively high-luminosity GRBs. In Section 4, first we derive an initial LF in both the BPL and SPLEC models by directly fitting the observational luminosity distribution of GRBs. Secondly, we analyse and constrain the so-called redshift-desert effect with the initial LFs. Finally, the combination of the above two processes gives a final constraint on the GRB LF, with which the prior selected luminosity threshold is checked. In Section 5, our conclusions and discussion are given.

2 BASIC CONSIDERATIONS

2.1 *Swift* observed GRBs

In the past few years, *Swift* has greatly promoted our understanding of GRBs. Here we take GRBs with measured redshift z from the *Swift* archive.[2] For most of these GRBs until GRB 090813, their spectral peak energy $E_{\rm p}$ and isotropically equivalent energy release $E_{\rm iso}$ in the burst rest-frame 1–10^4 keV band have been provided by Butler et al. (2007) and Butler, Bloom & Poznanski (2010). However, it should be noted that, due to the narrow energy bandpass of the *Swift* Burst Alert Telescope (BAT), the burst spectral parameters in Butler et al. (2007, 2010) are actually estimated by the Bayesian statistics, but not directly observed. Anyway, as in Kistler et al. (2008, 2009) and Wang & Dai (2009), an *average* luminosity can be roughly estimated for these GRBs by

$$L_{[1-10^4\,{\rm keV}]} = \frac{E_{{\rm iso}[1-10^4\,{\rm keV}]}}{T_{90}/(1+z)}. \quad (1)$$

In our statistics, GRBs with $L < 10^{49}$ erg s^{-1} will be excluded, since they may belong to a distinct population called low-luminosity GRBs (Soderberg et al. 2004; Cobb et al. 2006; Chapman et al. 2007; Liang et al. 2007). Finally, 125 GRBs are selected and their luminosity–redshift distribution is shown in Fig. 1. Correspondingly, including the GRBs without redshifts, there are in total 406 GRBs detected by *Swift* until GRB 090813.

[2] http://swift.gsfc.nasa.gov/docs/swift/archive/grb_table.

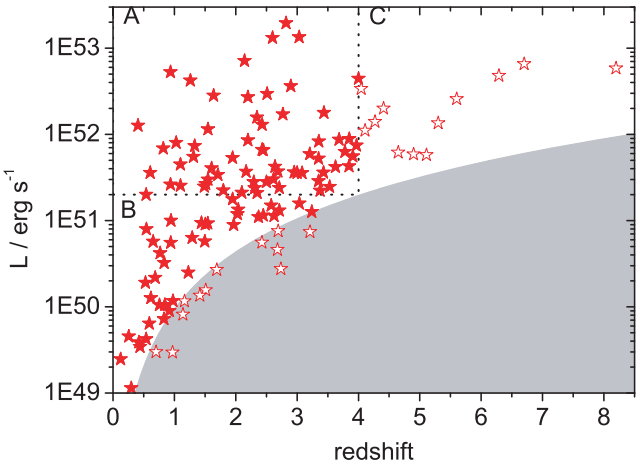

Figure 1. Luminosity–redshift distribution of 125 *Swift* GRBs with redshifts, where the shaded region represents the luminosity threshold adopted in our calculations (see equation 9 and explanations there). The 24 data shown by open stars will be excluded from our statistics except for in Fig. 2.

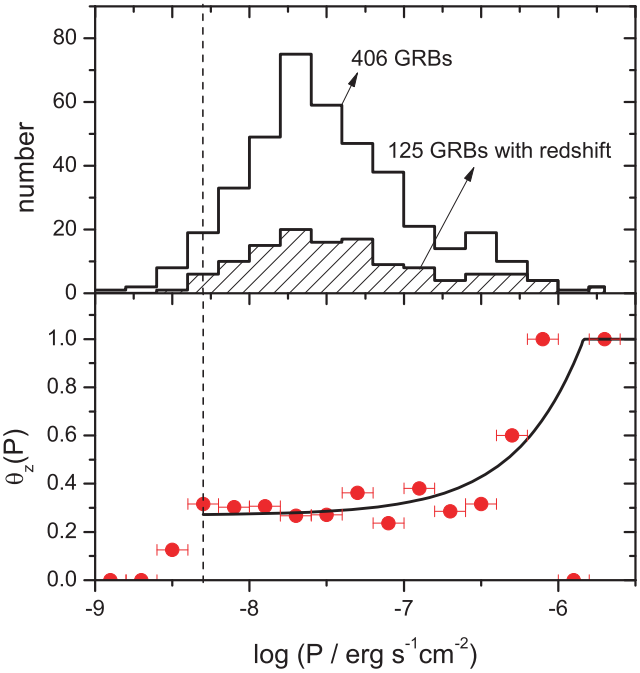

Figure 2. Upper panel: comparison between the distributions of average fluxes of all 406 GRBs and the 125 GRBs with redshifts. Lower panel: probability of redshift measurements as a function of flux and an empirical fit given by equation (2), where the horizontal error bars correspond to the bin width. The vertical dashed line represents the selected threshold $P_{\rm th} = 5 \times 10^{-9}$ erg s^{-1} cm^{-2}.

In the upper panel of Fig. 2, we present the distributions of the observed average fluxes,[3] $P_{[15-150\,{\rm keV}]}$, for both all 406 GRBs and the 125 GRBs with redshifts. The ratio between these two distributions generally displays the flux-dependence of the GRB redshift measurements and, as shown in the lower panel, such a

[3] The average fluxes are calculated from $S_{[15-150\,{\rm keV}]}/T_{90}$ where $S_{[15-150\,{\rm keV}]}$ is the observed fluence.

redshift detection probability can be empirically expressed by

$$\vartheta_z(P) = \min\left[0.27 + \frac{P}{2.0\times10^{-6}\,\mathrm{erg\,s^{-1}\,cm^{-2}}}, 1\right]. \quad (2)$$

A similar result has also been given by Qin et al. (2010). On the other hand, the redshift detection probability may also depend on the redshift itself, which will be investigated in Section 4.2.

2.2 Model

The luminosity–redshift distribution of GRBs is determined by both the LF $\phi(L)$ and the comoving rate $\dot{R}(z)$ of GRBs, which are respectively defined by

$$\frac{\mathrm{d}N}{\mathrm{d}L} = \phi(L) \quad (3)$$

and

$$\frac{\mathrm{d}\dot{N}}{\mathrm{d}z} = \dot{R}(z)\frac{\mathrm{d}V(z)/\mathrm{d}z}{1+z}, \quad (4)$$

where the dot represents time derivation, the factor $(1 + z)$ is due to the cosmological time dilation of the observed rate, and $\mathrm{d}V(z)/\mathrm{d}z$ is the comoving volume element. In the standard Λ cold dark matter cosmology, $\mathrm{d}V(z)/\mathrm{d}z = 4\pi d_c(z)^2 c/H(z)$ with $d_c(z) = d_l(z)/(1 + z)$, where the luminosity distance is $d_l(z) = c(1 + z)\int_0^z H(z')^{-1}\mathrm{d}z'$ with $H(z') = H_0[(1 + z')^3\Omega_{\mathrm{m},0} + \Omega_{\Lambda,0}]^{1/2}$. Throughout we adopt the cosmological parameters as $\Omega_{\mathrm{m},0} = 0.27, \Omega_{\Lambda,0} = 0.73$ and $H_0 = 71\,\mathrm{km\,s^{-1}\,Mpc^{-1}}$ (Komatsu et al. 2011).

First, the GRB rate $\dot{R}(z)$ can in principle be connected to the cosmic SFR $\dot{\rho}_*(z)$, since in the collapsar model the formation of each GRB just indicates the death of a short-lived massive star. For relatively low redshifts ($z < 4$), the SFR can be expressed approximately by (Hopkins & Beacom 2006)

$$\dot{\rho}_*(z) \propto \begin{cases} (1+z)^{3.44}, & z < 0.97, \\ (1+z)^{-0.26}, & 0.97 \le z < 4, \end{cases} \quad (5)$$

with $\dot{\rho}_*(0) = 0.02\,\mathrm{M_\odot\,yr^{-1}\,Mpc^{-3}}$, whereas the star formation history above $z \sim 4$ is unclear so far. So 12 GRBs with $z > 4$ (the data in region C in Fig. 1) are excluded from our statistics. Secondly, for the GRB LF, two representative forms are usually assumed in the literature: a BPL,

$$\phi(L) \propto \begin{cases} \left(\frac{L}{L_\mathrm{b}}\right)^{-\nu_1}, & L \le L_\mathrm{b}, \\ \left(\frac{L}{L_\mathrm{b}}\right)^{-\nu_2}, & L > L_\mathrm{b}, \end{cases} \quad (6)$$

and a SPLEC,

$$\phi(L) \propto \left(\frac{L}{L_\mathrm{p}}\right)^{-\nu} \mathrm{e}^{-L_\mathrm{p}/L}. \quad (7)$$

Then the expected number of GRBs with redshift $z_1 < z < z_2$ and luminosity $L_1 < L < L_2$ can be calculated by

$$N^{\mathrm{exp}} \propto \int_{z_1}^{z_2}\int_{\max[L_1, L_{\mathrm{th}}(z)]}^{L_2} (1+z)^{\Delta}\phi(L)\dot{\rho}_*(z)\,\mathrm{d}L\frac{\mathrm{d}V(z)}{1+z}, \quad (8)$$

where the extra evolving factor $(1+z)^\Delta$ is introduced by considering that (i) the connection between the GRB rate and the SFR may not be trivial; and (ii) the LF could evolve with redshift. Corresponding to different selection criteria and bin methods for different GRB samples, the specific form of the above equation (e.g. the sequence and the range of the integrals) should be changed: see equations (10), (11), (13), (15) and (18).

The luminosity threshold invoked in equation (8) can be given by

$$L_{\mathrm{th}}(z) = 4\pi d_l(z)^2 P_{\mathrm{th}} k(z), \quad (9)$$

where $k(z) \equiv \int_{1\,\mathrm{keV}}^{10^4\,\mathrm{keV}} S(E')E'\mathrm{d}E' / \int_{150(1+z)\,\mathrm{keV}}^{15(1+z)\,\mathrm{keV}} S(E')E'\mathrm{d}E'$ (the primes represent rest-frame energy) converts the observed flux in the BAT energy band 15–150 keV into the bolometric flux in the rest-frame $1-10^4$ keV. The observed photon number spectrum $S(E)$ can be well expressed by the empirical Band function (Band et al. 1993), more simply, a broken power law. The value of k varies from 5.4 to 2.1 as the redshift increases from 0 to 10, by taking the rest-frame peak energy as $E'_\mathrm{p} \sim 200\,\mathrm{keV}$ (the most frequent value in Butler et al.'s data base) and the photon indices prior- and post-break energy as 1 and 2.25, respectively (Preece et al. 2000). On the other hand, unfortunately, a precise description for P_{th} is nearly impossible, since the trigger of the BAT is very complicated and, especially for GRBs with redshifts, the actual threshold is determined by the combination of the BAT and other related telescopes. Instead of an abrupt cut-off at P_{th}, a realistic situation could be that the detection efficiency starts to significantly decrease at a certain flux and approaches zero with decreasing flux. Therefore, in the following calculations, a relatively high value for P_{th} is taken as $5\times10^{-9}\,\mathrm{erg\,s^{-1}\,cm^{-2}}$ and, correspondingly, 12 GRBs below the selected threshold are further excluded (as shown in Fig. 1). Strictly speaking, the selected P_{th} is not higher than the true sensitivity. This can help us to avoid the complexity arising from the trigger probability. The availability of the selected P_{th} will be checked by a fit to the $\log N - \log P$ distribution in Section 4.3.

2.3 Observational luminosity distribution

As our main objective, the luminosity distribution of the selected 101 GRBs (solid stars in Fig. 1) is presented in Fig. 3, where an obvious break appears at $\sim3\times10^{51}\,\mathrm{erg\,s^{-1}}$. Such a break may reflect an intrinsic break in the LF or just be caused by the selection effects arising from the BAT and also other related telescopes, which is what we want to clarify in this paper. In order to avoid consideration of the flux dependence of the redshift measurements in our analyses, an effective number as $\vartheta_z^{-1}(P)$ is defined for a redshift-known GRB whose flux is P. As a result, an effective GRB sample of about 319 is derived from the 101 GRBs. Since lower brightness

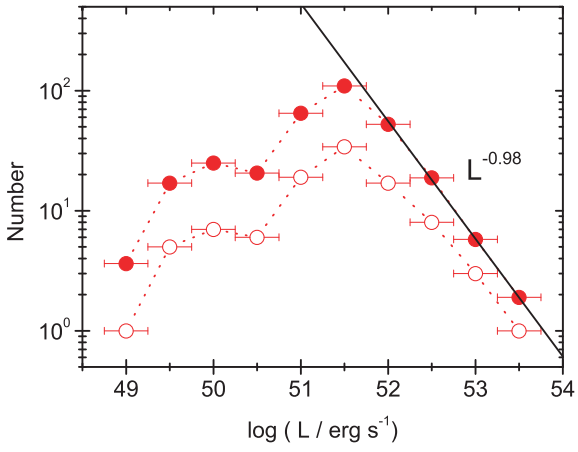

Figure 3. Luminosity distribution of the selected 101 GRBs, where the horizontal error bars correspond to the bin width. Open and solid circles correspond to pre- and post-corrected distributions, respectively, and the solid line gives a power-law fit for the corrected high-luminosity distribution. The equivalent number for the corrected sample is about 319.

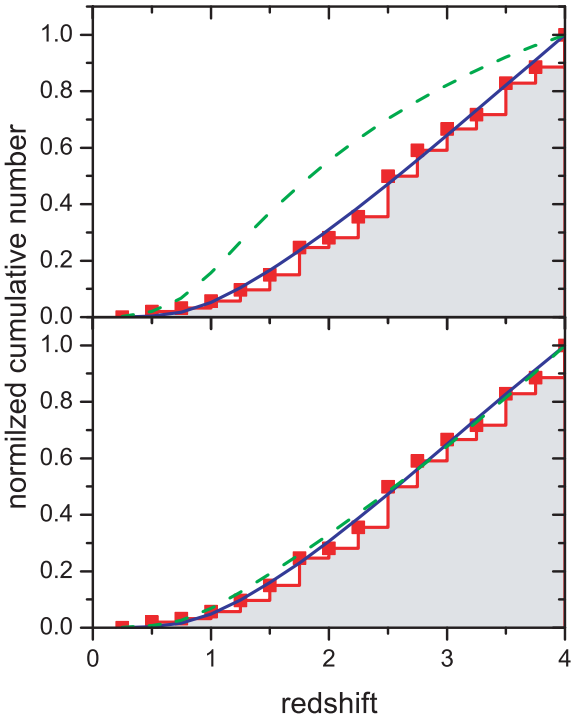

Figure 4. Normalized cumulative number of the 63 GRBs with $z < 4$ and $L > 2 \times 10^{51}$ erg s^{-1} as a function of redshift (histogram). Upper panel: fits to the redshift distribution with equation (10), where the solid and dashed lines correspond to $\Delta = 1.93$ and $\Delta = 0$, respectively. Lower panel: fits to the redshift distribution with equation (11), where the solid and dashed lines correspond to $Z_{\rm max} = 0.72\,Z_\odot$, $\delta = 1.56$ (best fit) and $Z_{\rm max} = 0.1\,Z_\odot$, $\delta = 0$, respectively.

GRBs have higher weight in the statistics, the corrected luminosity distribution becomes steeper, especially above the break luminosity. A good power-law fit as $N \propto L^{-0.98}$ to the high-luminosity distribution indicates $\nu_2 = 1.98$ in the BPL model and $\nu = 1.98$ in the SPLEC model, in view of the probable unimportance of most observational selection effects in the high-luminosity range. In the following Figs 4, 6, 7 and 8, the observational data all have the same number correction.

3 THE EVOLUTION EFFECT

Before we use the observational luminosity distribution to constrain the GRB LF with equation (8), we should determine the evolution parameter Δ in advance. Following Yüksel et al. (2008) and Kistler et al. (2009), the value of Δ can be constrained by fitting the observational cumulative redshift distribution of GRBs with relatively high luminosities ($L \geq L_{\rm cut}$). The cut luminosity $L_{\rm cut}$ is chosen to be equal to or higher than the threshold at the highest redshift of the sample (here $z_{\rm max} = 4$), so that, in the corresponding theoretical calculation, the integral of the LF can be treated as a constant coefficient no matter the specific form of the LF, i.e.

$$N_{<z}^{\rm exp} \propto \int_{L_{\rm cut}}^{L_{\rm max}} \phi(L){\rm d}L \int_0^z (1+z')^{\Delta} \dot{\rho}_*(z') \frac{{\rm d}V(z')}{1+z'}. \quad (10)$$

Due to the limited size of the sample, the observational redshift distribution actually is slightly dependent on the selected $L_{\rm cut}$. So we take $L_{\rm cut} = L_{\rm th}(4) = 2 \times 10^{51}$ erg s^{-1} to reduce the statistical uncertainty as much as possible. Consequently, 63 GRBs (the data in region A in Fig. 1) are selected. A comparison between the model and observations is presented in the upper panel of Fig. 4, which shows that the no-evolution case ($\Delta = 0$) can be definitely ruled out, as found before (e.g. Salvaterra & Chincarini 2007; Salvaterra et al. 2009; Kistler et al. 2008, 2009). The best fit to the observations gives $\Delta = 1.93$.[4]

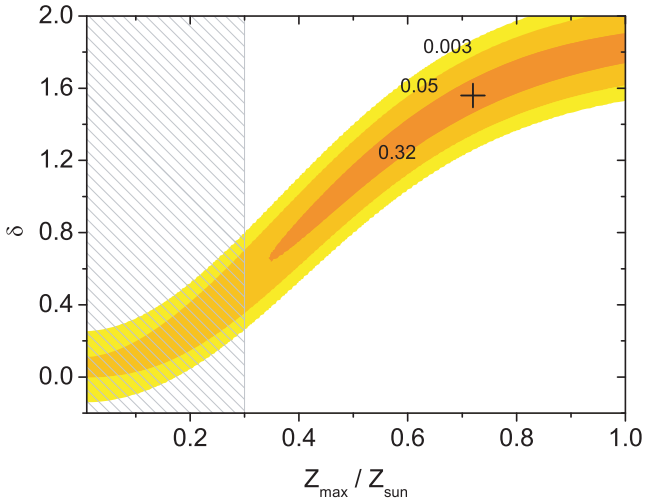

Figure 5. χ^2-probability distribution of the fits with equation (11) to the redshift distribution of the 63 GRBs with $z < 4$ and $L > 2 \times 10^{51}$ erg s^{-1}. The best-fitting parameters $\delta = 1.56$ and $Z_{\rm max} = 0.72\,Z_\odot$ are labelled by the cross. The hatched region represents the theoretical metallicity range expected by some collapsar models.

An interesting question then arises as to where such evolution comes from. As found by MacFadyen & Woosley (1999) and Yoon, Langer & Norman (2006), the formation of a black hole (or neutron star) during the collapse can drive a GRB event only if the collapsar has high angular momentum. In order to avoid strong stellar winds losing angular momentum, GRB progenitors are required to be in low-metallicity environments (Woosley & Heger 2006; Yoon et al. 2006). This theoretical metallicity requirement is widely favoured by the estimates of the metallicities of long GRB hosts (e.g. Chen et al. 2005; Gorosabel et al. 2005; Starling et al. 2005). Therefore, it is suggested that the observationally required evolution could be mainly due to the cosmic evolution of metallicity. Specifically, as derived by Langer & Norman (2006), the fraction belonging to metallicity below $Z_{\rm max}$ can be calculated by $\Psi_{<Z_{\rm max}}(z) = \hat{\Gamma}[0.84, (Z_{\rm max}/Z_\odot)^2 10^{0.3z}]/\Gamma(0.84)$, where $Z_{\rm max}$ is the maximum metallicity available for GRB progenitors, and $\hat{\Gamma}$ and Γ are the upper incomplete and complete gamma functions. Following this consideration, equation (10) becomes

$$N_{<z}^{\rm exp} \propto \int_{L_{\rm cut}}^{L_{\rm max}} \phi(L){\rm d}L \int_0^z (1+z')^{\delta} \Psi_{<Z_{\rm max}}(z') \dot{\rho}_*(z') \frac{{\rm d}V(z')}{1+z'}. \quad (11)$$

Varying the parameters $Z_{\rm max}$ and δ, we refit the observational redshift distribution shown in Fig. 4 and present the distribution of the χ^2-probabilities of the fits in Fig. 5. At first sight, the best-fitting parameters $Z_{\rm max} = 0.72\,Z_\odot$ and $\delta = 1.56$ may indicate that there is significant extra evolution other than the metallicity evolution. However, the long and narrow contours shown in Fig. 5 robustly demonstrate that the parameters $Z_{\rm max}$ and δ are actually strongly degenerate and, moreover, the specific values of the best-fitting parameters are probably sensitive to the selection of the observational

[4] If we do not correct the GRB number by the factor $\vartheta_z^{-1}(P)$, we can get $\Delta = 1.44$, which is consistent with the results in Kistler et al. (2008, 2009).

sample. Therefore, instead of paying attention to the best-fitting parameters, we treat the relationship between the two parameters exhibited by the contours as a more valuable result, very roughly, $\delta \sim 2.4(Z_{\rm max}/Z_\odot - 0.06)$. Anyway, an independent constraint on these two parameters is demanded in order to reduce the parameter degeneracy.

For example, a theoretical constraint on metallicity can be invoked (e.g. Campisi et al. 2010). As proposed by Woosley & Heger (2006) and Yoon et al. (2006), the maximum metallicity available for GRB progenitors is likely to be within $\sim[0.1-0.3]\,Z_\odot$. As shown in Fig. 5, for $Z_{\rm max} < 0.3\,Z_\odot$, the value of δ would not be higher than 0.8 with 99.7 per cent confidence. Especially for $Z_{\rm max} < 0.1\,Z_\odot$, the value of δ approaches zero. The fit to the observation with $Z_{\rm max} = 0.1\,Z_\odot$ and $\delta = 0$ is shown in the lower panel of Fig. 4 in comparison with the fit with $Z_{\rm max} = 0.72\,Z_\odot$ and $\delta = 1.56$. As can be seen, the difference between these two fits is not very significant. Therefore, extra evolution other than the metallicity evolution may be not inevitable if $Z_{\rm max}$ is indeed very low.

In the following calculations, we take the best-fitting parameters $Z_{\rm max} = 0.72$ and $\delta = 1.56$ just for a good description of the evolution effect. Constraints on the LF actually cannot be significantly affected by the variation of $Z_{\rm max}$ and δ as long as they satisfy the required relationship. On the other hand, for simplicity, we will ascribe the possible extra evolution to some unknown factors in the connection between the GRB rate and the SFR, i.e.

$$\dot{R}(z) = C_R(1+z)^{\delta}\Psi_{<Z_{\rm max}}(z)\dot{\rho}_*(z), \tag{12}$$

where the proportional coefficient C_R will be determined in Section 4.4. In other words, the LF will be taken to be non-evolving in this paper.

4 THE LUMINOSITY FUNCTION

4.1 A preliminary constraint

With given $Z_{\rm max}$ and δ, we can constrain the unknown LF by fitting the observational luminosity distribution of the 101 GRBs by

$$N^{\rm exp}_{[L_1,L_2]} \propto \int_{L_1}^{L_2}\int_0^{\min[z_M(L),4]} \phi(L)\dot{R}(z)\frac{{\rm d}V(z)}{1+z}\,{\rm d}L, \tag{13}$$

which gives the expected number in each luminosity bin $L_1 \le L \le L_2$. The maximum redshift $z_M(L)$ as a function of luminosity can be solved from[5]

$$\begin{aligned} d_{l,M}(L) &= \frac{c(1+z)}{H_0}\int_0^{z_M}\frac{1}{\sqrt{(1+z)^3\Omega_{\rm m,0}+\Omega_{\Lambda,0}}}{\rm d}z \\ &= \left(\frac{L}{4\pi P_{\rm th}k}\right)^{1/2}. \end{aligned} \tag{14}$$

With fixed $\nu_2 = 1.98$ in the BPL model, and $\nu = 1.98$ in the SPLEC model, and minimizing the χ^2-statistic of the fits, we obtain the best-fitting parameters as $L_{\rm b} = 2.5\times10^{52}\,{\rm erg\,s^{-1}}$ and $\nu_1 = 1.67$ for the BPL model, and $L_{\rm p} = 2.5\times10^{49}\,{\rm erg\,s^{-1}}$ for the SPLEC model. As shown in Fig. 6, the fit with a BPL LF seems much better than the one with a SPLEC LF. This impels us to favour the BPL model. However, the apparent oscillation of the observational data, which cannot be explained by either model, still demands a much more elaborate fit.

[5] With an approximate expression for luminosity distance as $d_l(z) \approx \frac{3c}{H_0}\sqrt{1+z}(\sqrt{1+z}-1)$, the maximum redshift can be approximately calculated by $z_M \approx \frac{1}{2}(\sqrt{1+4H_0d_{l,M}/3c}+2H_0d_{l,M}/3c-1)$.

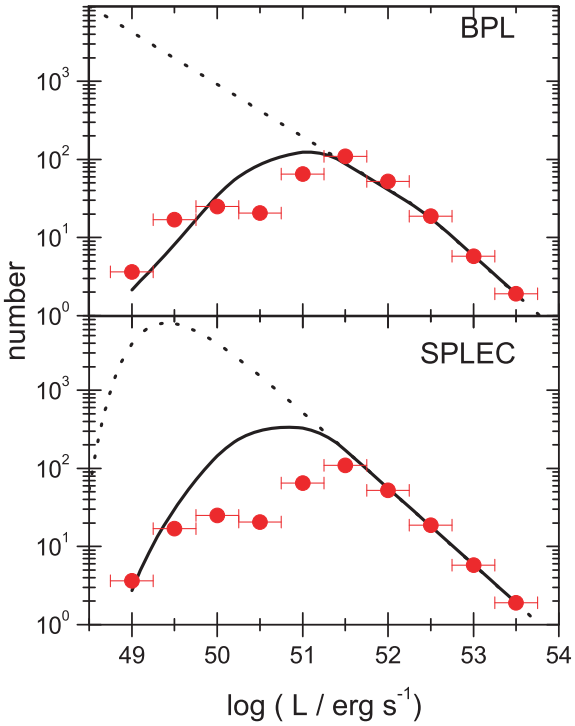

Figure 6. The best fit to the observational GRB luminosity distribution with equation (13). The dotted and solid lines represent intrinsic and observable distributions, respectively. The parameters are $L_{\rm b} = 2.5\times10^{52}\,{\rm erg\,s^{-1}}$, $\nu_1 = 1.67$ and $\nu_2 = 1.98$ for the BPL model (upper), and $L_{\rm p} = 2.5\times10^{49}\,{\rm erg\,s^{-1}}$ and $\nu = 1.98$ for the SPLEC model (lower).

4.2 Redshift-desert effect

With the preliminary LFs derived above, we can give some model-predicted cumulative redshift distributions by

$$N^{\rm exp}_{<z} \propto \int_0^z\int_{L_{\rm th}(z)}^{L_{\rm max}} \phi(L)\dot{R}(z')\,{\rm d}L\frac{{\rm d}V(z')}{1+z'}, \tag{15}$$

which are shown in the upper panel of Fig. 7 in comparison with the observational one of the 101 GRBs. Obviously, the observational numbers at middle redshifts are much lower than those predicted by both models. Such a remarkable dip in the observational redshift distribution is probably, at least partly, related to the so-called 'redshift-desert' effect, which is ignored in the above analyses. As qualitatively analysed by Fiore et al. (2007), it could be difficult to measure redshifts within the range $1.1 < z < 2.1$, since at $z > 1.1$ some strong observable emission or absorption lines are shifted outside the typical interval covered by optical spectrometers (3800–8000 Å), while Lyman α enters the range at $z \sim 2.1$. In this paper we do not try to give a theoretical description for the redshift-desert effect, which must involve many physical and technical issues. We also notice that the same significant dip actually cannot be found in the redshift distribution of only GRBs with $L > 2\times10^{51}\,{\rm erg\,s^{-1}}$, as shown in Fig. 4. Hence, we suspect that the redshift-desert effect may mainly influence the redshift measurements of relatively low-brightness GRBs, which can also be implied by the luminosity distribution.

Therefore, we show the observational redshift distribution of only 38 GRBs with $z < 4$ and $L < 2\times10^{51}\,{\rm erg\,s^{-1}}$ (the data in region B in Fig. 1) in the lower panel of Fig. 7. Meanwhile, for relatively

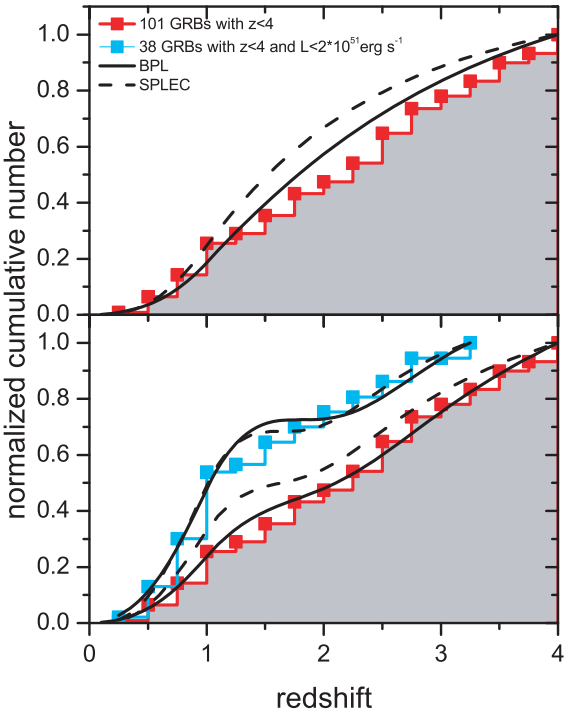

Figure 7. Model-predicted redshift distributions with (upper) and without (lower) the redshift-desert effect in comparison with the observational distribution, where the adopted LFs are the same as in Fig. 6. The parameters for the redshift-desert effect are $\mu = 1.80$ and $\sigma = 0.56$ for the BPL model, and $\mu = 1.63$ and $\sigma = 0.43$ for the SPLEC model.

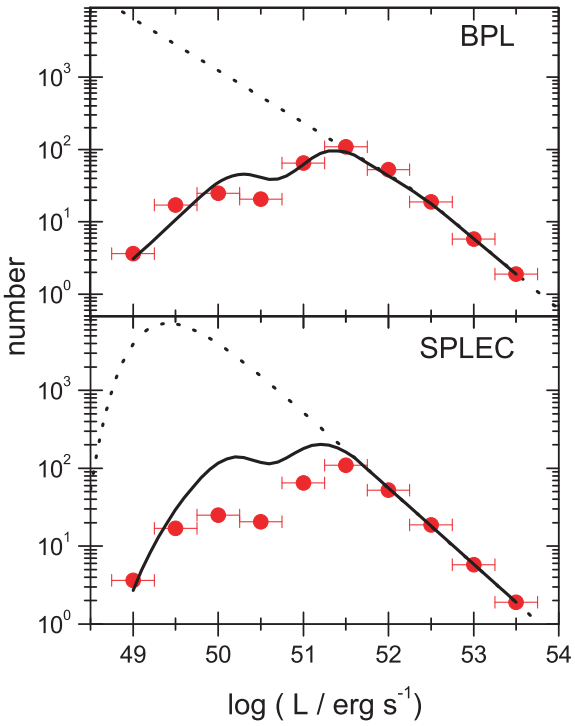

Figure 8. The same as Fig. 6 but with a redshift-desert effect derived from Fig. 7. The LF parameters are $L_{\rm b} = 2.5 \times 10^{52}\,{\rm erg\,s^{-1}}$, $\nu_1 = 1.72$ and $\nu_2 = 1.98$ for the BPL model, and $L_{\rm p} = 2.5 \times 10^{49}\,{\rm erg\,s^{-1}}$ and $\nu = 1.98$ for the SPLEC model.

low-brightness GRBs, we tentatively suggest a function

$$\eta_z(z) = 1 - \exp\left[-\frac{(z-\mu)^2}{2\sigma^2}\right] \tag{16}$$

to phenomenologically describe the redshift-dependence of the redshift measurements. In contrast, for sufficiently bright GRBs, we take

$$\eta_z(z) = 1. \tag{17}$$

Fits to the distribution of the 38 GRBs give the best-fitting parameters as $\mu = 1.80$ and $\sigma = 0.56$ for the BPL model and $\mu = 1.63$ and $\sigma = 0.43$ for the SPLEC model, which are basically consistent with the theoretical expectation of the redshift-desert effect. With these phenomenological expressions of $\eta_z(z)$, we refit the redshift distribution of the 101 GRBs, which is also shown in the lower panel of Fig. 7. As can be seen, the fits are greatly improved, as the observational dip in the redshift distribution is produced naturally, especially in the BPL model.

4.3 Final results

Combining equations (13), (16) and (17), we refit the luminosity distribution of the 101 GRBs and find that $L_{\rm b} = 2.5 \times 10^{52}\,{\rm erg\,s^{-1}}$ and $\nu_1 = 1.72$ for the BPL model, and $L_{\rm p} = 2.5 \times 10^{49}\,{\rm erg\,s^{-1}}$ for the SPLEC model. Strictly, we should use these new LFs to re-constrain the redshift-desert effect and continue the cycle until we reach a certain precision. For simplicity, we stop here because the obtained new values of the parameters are only slightly different from the preliminary ones. With these new parameters, Fig. 8 shows that the BPL model agrees with the observation successfully, whereas the SPLEC model still predicts some remarkable excesses around $\sim 10^{50}$–$10^{51}\,{\rm erg\,s^{-1}}$. Therefore, we prefer to conclude that the GRB LF could be a BPL.

Finally, with the derived BPL LF, we give a model-predicted cumulative flux distribution by

$$N_{>P}^{\rm exp} \propto \int_0^4 \int_{L_P}^{L_{\rm max}} \phi(L)\dot{R}(z)\vartheta_z(P')\eta_z(z)\,{\rm d}L\,\frac{{\rm d}V(z)}{1+z}, \tag{18}$$

where $L_P = 4\pi d_l^2 kP$, $P' = L/4\pi d_l^2 k$, and the redshift detection probability $\vartheta_z(P')\eta_z(z)$ has been determined above. As shown in Fig. 9, the consistency between the theoretical and observational flux distributions indicates that our choice of the luminosity threshold is

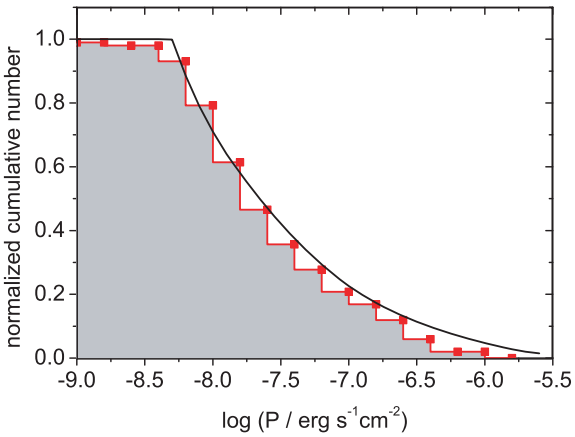

Figure 9. Comparison of the model-predicted flux distribution in the BPL LF model with the observational one (without number correction) of the 101 GRBs. The model parameters are the same as in Fig. 8.

basically reasonable, i.e. the trigger probability above $P_{\rm th}$ by the BAT can be confirmed to be nearly constant.

4.4 GRB rate

In the above fits to the luminosity distribution, we normalize the model-predicted GRB number by the following equation:[6]

$$N^{\rm obs}_{[53.25,53.75]} = \frac{\Delta\Omega}{4\pi} T f_{\rm b} \int_{10^{53.25}}^{10^{53.75}} C_L \phi(L) {\rm d}L \int_0^4 \dot{R}(z) \frac{{\rm d}V(z)}{1+z}. \quad (19)$$

where $(\Delta\Omega/4\pi) \sim 0.1$ is the field of view of the BAT, $T \sim 5$ yr is the observational period, $f_{\rm b} \sim 0.01$ is the beaming degree of the GRB outflow, and $C_L \approx (\nu_1 - 1)(\frac{L_{\rm min}}{L_{\rm b}})^{\nu_1 - 1} \frac{1}{L_{\rm b}}$ is the normalization coefficient of the BPL LF with $L_{\rm min}$ being an assumed minimum luminosity for the GRBs.

For $\delta = 1.56$, $Z_{\rm max} = 0.72\,{\rm Z}_\odot$, $\nu_1 = 1.72$, $\nu_2 = 1.98$, $L_{\rm b} = 2.5 \times 10^{52}\,{\rm erg\,s^{-1}}$ and $N^{\rm obs}_{[53.25,53.75]} = 1.9$, the proportional coefficient in the GRB rate can be constrained to

$$C_R = 8 \times 10^{-6} \left(\frac{L_{\rm min}}{10^{-4} L_{\rm b}}\right)^{1-\nu_1} \left(\frac{f_{\rm b}}{0.01}\right)^{-1} {\rm M}_\odot^{-1}, \quad (20)$$

which yields an overall local GRB rate as $\dot{R}(0) = C_R \Psi_{<Z_{\rm max}}(0) \dot{\rho}_*(0) = 74 (f_{\rm b}/0.01)^{-1}\ {\rm Gpc^{-3}\,yr^{-1}}$ and an observed local GRB rate as $f_{\rm b}\dot{R}(0) = 0.74\ {\rm Gpc^{-3}\,yr^{-1}}$. This rate is basically consistent with the previous results (e.g. Schmidt 2001; Guetta et al. 2004, 2005; Liang et al. 2007; Wanderman & Piran 2010). The value of C_R also implies that, besides the metallicity requirement, GRB progenitors may also have some other particular properties. For example, as widely accepted, only massive Wolf–Rayet stars (e.g. $>20\,{\rm M}_\odot$) are possible GRB progenitors (MacFadyen & Woosley 1999; Larsson et al. 2007). So a small fraction arise as $f_{\rm WR} = \int_{20\,{\rm M}_\odot}^{100\,{\rm M}_\odot} \varphi(m){\rm d}m / \int_{0.1\,{\rm M}_\odot}^{100\,{\rm M}_\odot} m\varphi(m){\rm d}m \approx 2 \times 10^{-3}\ {\rm M}_\odot^{-1}$, where $\varphi(m)$ is the Salpeter initial stellar mass function. Additionally, there is still an extra factor of $\sim 10^{-3}$–10^{-2} unexplained, which could be related to the particular property of GRB progenitors in their rotation, magnetic fields, etc. The specific value of this extra factor is dependent on the choice of $Z_{\rm max}$.

5 CONCLUSION AND DISCUSSION

The accumulation of *Swift* observed GRBs has gradually made it possible to derive a GRB LF directly from the observational luminosity distribution. However, two complexities must be involved: (i) the evolving connection between the GRB rate and the cosmic SFR; and (ii) observational selection effects. With a phenomenological investigation of these two complexities, we constrain and discriminate two popular competing LF models and find that the BPL LF model is more favoured by the observations. However, in view of the approximate description of the selection effects, the SPLEC model still cannot be ruled out absolutely.

Although the derived values of the parameters μ and σ are basically consistent with the theoretical expectation of the redshift-desert effect, the flux dependence of the redshift-desert effect is still very ambiguous (an abrupt luminosity boundary of $2 \times 10^{51}\,{\rm erg\,s^{-1}}$ is adopted in our analyses). More seriously, the flux and redshift dependences of the redshift measurements actually must be coupled with each other, but in our analyses the functions $\vartheta_z(P)$ and $\eta_z(z)$ are considered independently for simplicity. This may lead to an overestimation of the redshift selection effect. Therefore, some more elaborate theoretical considerations of the redshift measurements are demanded. On the other hand, of course, a more detailed analysis of the observational results would be helpful, especially regarding redshift measurement methods.

Finally, our investigation of the evolution effect shows that, if the metallicity of GRB progenitors is lower than $\sim 0.1\,{\rm Z}_\odot$ as expected by some collapsar models, there may be no extra evolution effect (i.e. $\delta \sim 0$) other than the metallicity evolution. Alternatively, if we remove the theoretical metallicity requirement, stronger extra evolution would be required for higher metallicities. In the latter case, the extra evolution could indicate some other evolution in the GRB rate, or indicate an evolving LF which is not considered in this paper. To discriminate between these two possibilities is difficult but interesting. It will be helpful to separate the GRB sample into a few subsamples with different redshift ranges and fit the luminosity distribution of each subsample one by one with an evolving LF. Such further work can be done when the GRB sample becomes large enough.

[6] The normalization is usually estimated with an entire data set or a good statistical point. Here, we select the data at the highest luminosity $L = 10^{53.5}\,{\rm erg\,s^{-1}}$ for normalization for two reasons: (i) the data above $L = 10^{52}\,{\rm erg\,s^{-1}}$ can be well fitted by a power law, which indicates that all the data above $L = 10^{52}\,{\rm erg\,s^{-1}}$ are probably good statistically; and (ii) more higher-luminosity GRBs may have fewer selection effects.

ACKNOWLEDGMENTS

We acknowledge the use of public data from the *Swift* data archive and thank D. Yonetoku for his invaluable comments and suggestions which have significantly improved our work. This work is supported by the National Natural Science Foundation of China (grant nos 11047121 and 11103004) and by the Self-Determined Research Funds of CCNU (grant no. CCNU09A01020) from the Colleges' Basic Research and Operation of MOE of China. X-FC is supported by the Scientific Innovation Foundation of CCNU. KSC is supported by the GRF Grants of the Government of the Hong Kong SAR under HKU7011/09P.

REFERENCES

Band D. et al., 1993, ApJ, 413, 281
Butler N. R., Kocevski D., Bloom J. S., Curtis J. L., 2007, ApJ, 671, 656
Butler N. R., Bloom J. S., Poznanski D., 2010, ApJ, 711, 495
Campisi M. A., Li L.-X., Jakobsson P., 2010, MNRAS, 407, 1972
Chapman R., Tanvir N. R., Priddey R. S., Levan A. J., 2007, MNRAS, 382, L21
Chen H.-W., Prochaska J. X., Bloom J. S., Thompson I. B., 2005, ApJ, 634, L25
Chornock R. et al., 2010, ApJL, submitted (arXiv:1004.2262)
Cobb B. E., Bailyn C. D., van Dokkum P. G., Natarajan P., 2006, ApJ, 645, L113
Cucchiara A. et al., 2011, ApJ, 736, 7
Daigne F., Rossi E. M., Mochkovitch R., 2006, MNRAS, 372, 1034
Fenimore E. E., Ramirez-Ruiz E., 2000, arXiv:astro-ph/0004176
Fiore F., Guetta D., Piranomonte S., D'Elia V., Antonelli L. A., 2007, A&A, 470, 515
Firmani C., Avila Reese V., Ghisellini G., Tutukov A. V., 2004, ApJ, 611, 1033
Fryer C. L., Woosley S. E., Hartmann D. H., 1999, ApJ, 526, 152
Gehrels N. et al., 2004, ApJ, 611, 1005
Gorosabel J. et al., 2005, A&A, 444, 711
Guetta D., Perna R., Stella L., Vietri M., 2004, ApJ, 615, L73
Guetta D., Piran T., Waxman E., 2005, ApJ, 619, 412
Hjorth J. et al., 2003, Nat, 423, 847
Hopkins A. M., Beacom J. F., 2006, ApJ, 651, 142

Kistler M. D., Yüksel H., Beacom J. F., Stanek K. Z., 2008, ApJ, 673, L119
Kistler M. D., Yüksel H., Beacom J. F., Hopkins A. M., Wyithe J. S. B., 2009, ApJ, 705, 104
Komatsu E. et al., 2011, ApJS, 192, 18
Langer N., Henkel C., 1995, Space Sci. Rev., 74, 343
Langer N., Norman C. A., 2006, ApJ, 638, L63
Larsson J., Levan A. J., Davies M. B., Fruchter A. S., 2007, MNRAS, 376, 1285
Liang E., Zhang B., Virgili F., Dai Z. G., 2007, ApJ, 662, 1111
MacFadyen A. I., Woosley S. E., 1999, ApJ, 524, 262
Meynet G., Maeder A., Schaller G., Schaerer D., Charbonnel C., 1994, A&AS, 103, 97
Natarajan P., Albanna B., Hjorth J., Ramirez-Ruiz E., Tanvir N., Wijers R., 2005, MNRAS, 364, L8
Paczyński B., 1998, ApJ, 494, L45
Porciani C., Madau P., 2001, ApJ, 548, 522
Preece R. D., Briggs M. S., Mallozzi R. S., Pendleton G. N., Paciesas W. S., Band D. L., 2000, ApJS, 126, 19
Qin S. F., Liang E. W., Lu R. J., Wei J. Y., Zhang S. N., 2010, MNRAS, 406, 558
Salvaterra R., Chincarini G., 2007, ApJ, 656, L49
Salvaterra R., Guidorzi C., Campana S., Chincarini G., Tagliaferri G., 2009, MNRAS, 396, 299
Schmidt M., 1999, ApJ, 523, L117
Schmidt M., 2001, ApJ, 552, 36
Soderberg A. M. et al., 2004, Nat, 430, 648
Stanek K. Z. et al., 2003, ApJ, 591, L17
Starling R. L. C. et al., 2005, A&A, 442, L21
Vink J. S., de Koter A., 2005, A&A, 442, 587
Wanderman D., Piran T., 2010, MNRAS, 406, 1944
Wang F. Y., Dai Z. G., 2009, MNRAS, 400, L10
Wheeler J. C., Yi I., Höflich P., Wang L., 2000, ApJ, 537, 810
Woosley S. E., 1993, ApJ, 405, 273
Woosley S. E., Bloom J. S., 2006, ARA&A, 44, 507
Woosley S. E., Heger A., 2006, ApJ, 637, 914
Yonetoku D., Murakami T., Nakamura T., Yamazaki R., Inoue A. K., Ioka K., 2004, ApJ, 609, 935
Yoon S.-C., Langer N., Norman C., 2006, A&A, 460, 199
Yüksel H., Kistler M. D., Beacom J. F., Hopkins A. M., 2008, ApJ, 683, L5

This paper has been typeset from a TEX/LATEX file prepared by the author.